GEOPHYSICS, VOL. 82, NO. 2 (MARCH-APRIL 2017); P. B49–B61, 18 FIGS., 2 TABLES.
10.1190/GEO2016-0103.1

Case History

Modeling induced polarization effects in helicopter time-domain electromagnetic data: Field case studies

Vladislav Kaminski[1] and Andrea Viezzoli[1]

ABSTRACT

Induced polarization (IP) effects are becoming more evident in time-domain helicopter airborne electromagnetic (AEM) data thanks to advances in instrumentation, mainly due to improvements in the signal-to-noise ratio and hence better data quality. Although the IP effects are often manifested as negative receiver voltage values, which are easy to detect, in some cases, IP effects can distort recovered transients in other ways so they may be less obvious and require careful data analysis and processing. These effects represent a challenge for modeling and inversion of the AEM data. For proper modeling of electromagnetic transients, the chargeability of the subsurface and other parameters describing the dispersion also need to be taken into consideration. We use the Cole-Cole model to characterize the dispersion and for modeling of the IP effects in field AEM data, collected by different airborne systems over different geologies and exploration targets, including examples from diamond, gold, and base metal exploration. We determined how multiparametric inversion techniques can simultaneously recover all four Cole-Cole parameters, including resistivity ρ, chargeability m_0, relaxation time τ, and frequency parameter c. The results obtained are in good agreement with the ancillary information available. Interpretation of the IP effects in AEM data is therefore seen by the authors as providing corrected electrical resistivity distributions, as well as additional information that could assist in mineral exploration.

INTRODUCTION

Interest in the impact of induced polarization (IP) effects on airborne electromagnetic (AEM) data has significantly increased over the past several years (Viezzoli et al., 2016). This interest results from an increased incidence of reverse-sign (negative) voltage anomalies, which is primarily attributed to better signal-to-noise performance of most airborne time-domain electromagnetic (TDEM) systems, more advanced data processing, and improved modeling and computational capabilities (Prikhodko et al., 2010). However, some data providers extract chargeabiity information from AEM data without providing reference to the depth of its possible distribution (Chen et al., 2015; Kwan et al., 2015). In other recent research, it has been suggested that commonly used AEM systems are likely to show limited sensitivity to chargeable targets at depths in excess of the first dozens of meters (Macnae, 2015a).

The negative voltage values are obvious in the data; however, more subtle airborne induced polarization (AIP) effects may be difficult to identify. Failing to recognize and properly model these effects during inversion can sometimes either lead to difficulties in accurate fitting of the data or, worse, to severe artifacts in the derived electrical resistivity/conductivity models.

This paper presents some practical examples derived from processing and modeling of the AIP effect from four heliborne TDEM case studies. The data were acquired with different geophysical systems, in different geologies, and over different mineral exploration targets. These results may be seen as a logical follow-up to the synthetic modeling exercises presented in Viezzoli et al. (2016). Together, these two papers will contribute to better establishing the actual relevance and applicability of the multiparametric inversion approach in the industry and the potential to improve recovery of physical parameters.

Manuscript received by the Editor 26 February 2016; revised manuscript received 12 August 2016; published online 30 January 2017.
[1]Aarhus Geophysics, Aps, Risskov, Denmark. E-mail: kam3000@gmail.com; andrea.viezzoli@aarhusgeo.com.

The physics of the AIP effect in TDEM have been described in the literature in the past (Pelton et al., 1978; Smith and West, 1988; Flis et al., 1989; Smith and Klein, 1996; Viezzoli et al., 2013). It has been widely accepted in ground TDEM data (Kamenetsky et al., 2014); however, in airborne data, the IP effects are increasingly evident and can be attributed to the same physical phenomena. The AIP effects in TDEM data can be described with an equation introduced by Cole and Cole (1942):

$$\zeta(\omega) = \rho\left[1 - \frac{m_0}{10^3}\left(1 - \frac{1}{1 + (i\omega\tau)^C}\right)\right], \tag{1}$$

where there are four interconnected parameters (ρ: electrical resistivity, ohm-m; m_0: chargeability, mV/V; τ: relaxation constant, s; and c: frequency parameter). These parameters play an important role in determining the transient decays in airborne TDEM data in the presence of chargeable media. The polarization currents can be comparable with the induction currents, either creating abnormal variations in the observed time-domain decay curves (Figure 1) or sometimes forcing the measured voltages to become negative (when the rate of change of the reversed IP currents exceeds the rate of change of the induction currents).

The Cole-Cole model can be expressed either in its low-frequency-limit version (as suggested in this paper) or in the high-frequency limit. Flis et al. (1989) and Smith (1989) provide a very insightful discussion on whether the IP effects in AEM data are more correctly described using the low- or high-frequency limit. One of the main differences is that in Flis et al. (1989), the polarization currents initially oppose the purely inductive currents, whereas in Smith (1989), they always oppose it. Despite this difference, both approaches account for an increase in the measured voltage in transients at very early times and converge to the same transient at intermediate to late times. In our view, both approaches are potentially valid, but we have adopted the low-frequency limit version due to some modeling considerations used in the "AarhusINV" code (Fiandaca et al., 2012).

The low- and high-frequency parameterized Cole-Cole IP models equally fit the spectral IP data. Any two of ρ_0, ρ_∞, or m_0 are identical in their ability to fit data. The same c value applies to both models, but the resistivity formulation leads to a slightly different time constant (Tarasov and Titov, 2013; Macnae, 2015c). Notwithstanding this choice, we expect that the main results and discussions presented in this paper would remain valid also for the high-frequency limit approach.

METHODOLOGY

From our experience, even in the absence of IP effects, proper modeling of AEM data can only be achieved by applying a carefully customized workflow. The following are the steps of the workflow undertaken in all the case studies presented in this paper: From our experience, even in the absence of IP effects, proper modeling of AEM data can only be achieved by applying a carefully customized workflow. The following are the steps of the workflow undertaken in all the case studies presented in this paper:

1) Understanding the AEM data: The workflow starts with gathering all information about the preprocessing carried out by the contractors, to ensure that the applied filtering routines did not significantly alter the raw data either by masking the IP effect or by introducing "IP-like" artifacts. For example, some forms of TEMPEST processing fit positive exponentials to the data (Lane et al., 2000) and remove all negatives. The transients displayed in Figure 1 include raw (green) and processed (blue) and show either no sign change (Figure 1b and 1e), or a single sign change (Figure 1a, 1d, and 1f), or a double sign change (Figure 1c and 1g). From this collection, only those transients, showing a double sign change would be treated as obvious IP effects; the ones with a single sign change may or may not be related to system calibration problems or incorrect altitude testing (preprocessing), and those with no sign change would be hard to interpret as IP effects, unless looked at by an experienced data processor.
2) Manual data processing: A thorough visual inspection of the profile data is carried out, assessing and editing the "raw" electromagnetic (EM) transients (Figures 1 and 2). This is a fundamental step for several reasons:
   - The IP effects are not very easily recognized by visual inspection of gridded 2D maps of individual time channels. For example, they are not necessarily associated with negative voltage values. Viezzoli et al. (2016) present a wide variety of IP signatures in synthetic data,

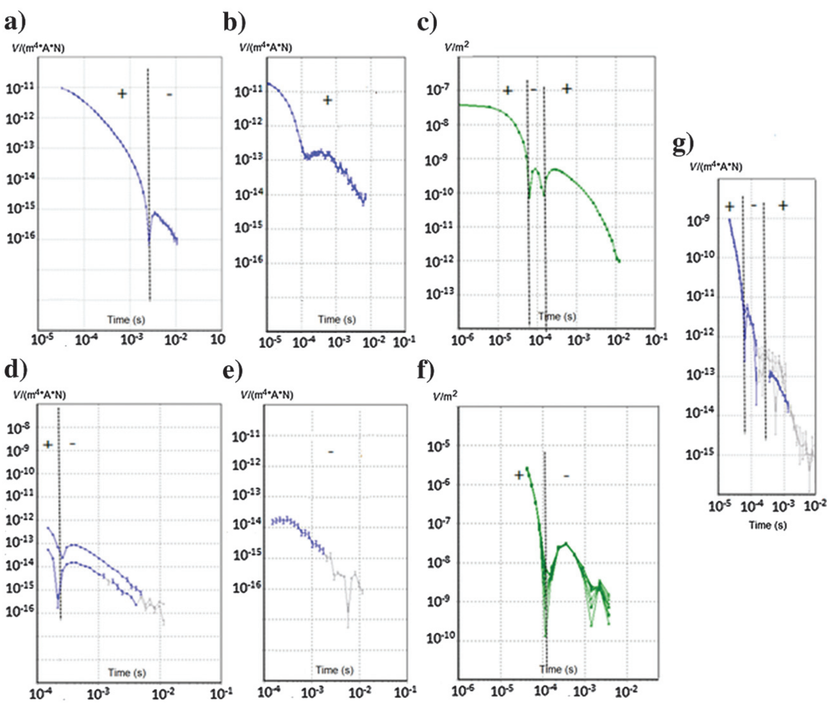

Figure 1. Transients with IP effects. (a) VTEM example (single sign change). (b) VTEM example (no sign change). (c) VTEM example (double sign change). (d) SkyTEM example (single sign change). (e) HeliTEM example (all negative). (f) Equator example (single sign change). (g) HeliTEM example (double sign change).

such as abnormally rapid decay in transients, as well as other types of deviation from normal transient voltage behavior. Similar signatures may be found in field data (Prikhodko et al., 2010; Viezzoli and Kaminski, 2016). Figures 1 and 2 show examples of IP effects, as recorded in actual field transients, measured by different airborne TDEM systems.

- It is important to establish a preliminary classification, in which more obvious IP signatures present in the data sets become evident. We have found that even the most obvious manifestations of IP effect vary across different geologic domains and therefore show distinctive features specific to these domains. This information is relevant to the next step: the modeling. Examples of different IP signatures over different geologies from a versatile time domain electromagnetic (VTEM) survey, flown in the Northern Territories (Australia) are shown in Figure 3. In this figure, different rock types are responsible for different IP effect signatures with one corresponding to alluvium, two corresponding to schist, and three corresponding to granite. In addition, all transients in Figure 3 show positive voltages in early times, which then turn negative toward later times. It is remarkable how the sign reversal migrates from earlier to later times over a single line, depending on the different geologies and, therefore, different Cole-Cole parameter values, causing the IP effects.
- When the EM signal is clearly less than random noise, these data should be excluded from any further processing, while retaining the IP effects when possible. Often, with the IP effect manifested in later time gates in some transients, such differentiation becomes very dependent on the user's experience and understanding of the data and the steps taken to deliver the data. In addition, IP effects may differ in shape and amplitude, as well as may affect different time gates. Based on our experience, it is virtually impossible to separate the IP effect from noise using automatic algorithms or constant noise floors. In Viezzoli et al. (2016), such a manual editing approach was tested on synthetic data and showed positive results. As a result, similar manual noise editing techniques were applied to field data and are shown in Figures 4 and 5.

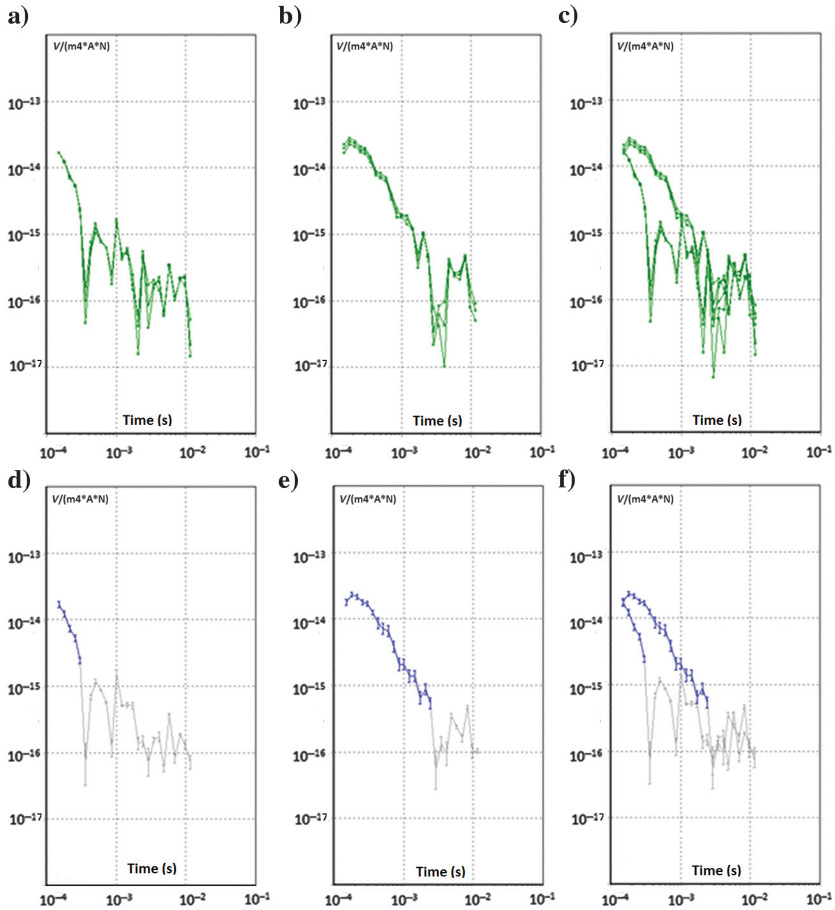

Figure 2. Examples of manual processing of selected HeliTEM sets of transients. (a) Set 1 before manual processing. (b) Set 2 before manual processing. (c) Sets 1 and 2 before manual processing imaged together. (d) Set 1 after manual data processing. (e) Set 2 after manual data processing. (f) Sets 1 and 2 after manual data processing imaged together.

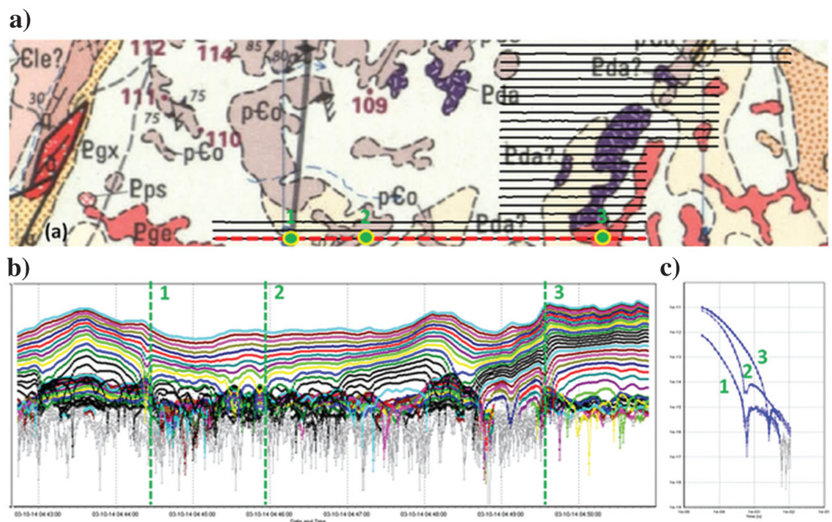

Figure 3. A single VTEM profile (1330), showing different types of IP effects produced by different geologic features. (a) Geologic units intercepted by a VTEM flight line, (b) VTEM flight line data with three notable IP effects, and (c) individual VTEM transients extracted from profile data and corresponding to the locations marked on the geologic map.

In Figure 4, the part of the section that shows strong negative values in late times is circled in a dashed blue line, whereas the raw and processed transients (Figure 4b and 4c) are entirely positive. In Figure 5, it should be noted that the transients at approximately 00:48 are entirely negative.

- The quality of data processing delivered by a contractor may subsequently require additional "preinversional" improvement, including manual data processing based on the considerations described above.

We suggest that this step should be carried out manually. Macnae et al. (1984) provide a comprehensive review of different noise sources in AEM data. In our approach, any part of the measured signal that can be associated with anything other than the secondary magnetic field induced in the ground by the AEM transmitter is defined as noise. Noise can be divided into two different components: coherent noise (e.g., coupling with infrastructures or individual sferics) and random noise (e.g., the background response of the earth). In our approach, the coherent noise is eliminated by deleting full transients, whereas the random noise is first reduced by stacking, and then it is eliminated from the transient if it exceeds actual ground response. One fundamental issue in assessing noise in an AEM transient is that noise is very rarely measured directly, but in most cases it is derived from the data. This implies that postprocessing routines applied to the AEM data (e.g., leveling) can affect our ability to assess noise. The procedure for culling background noise, which is used in the case studies described in this paper, is adapted from Auken et al. (2009). It can be shown that the background noise decreases with $t^{-1/2}$ in transients that deploy the logarithmic gating scheme (i.e., the width of the time gates increases logarithmically with time). This is confirmed by visual analysis of the envelope of a few raw transients. Late-time background noise can be reduced to some degree by stacking/lateral averaging of adjacent transients. However, depending on the geology and AEM system characteristics, it often persists at the late times. If not removed before inversion, it can produce artifacts in the model space (Viezzoli et al., 2012). Even though, in principle, it is possible to use a constant noise floor for automated culling of background noise, our experience (Viezzoli et al., 2012) shows that the noise levels that contaminate the recorded ground response can vary during a survey. We therefore prefer adopting a staged approach. We first apply automated filtering, but then we follow it inspecting the raw transient data visually, reassessing which part of the transients are affected by background noise, and refine the culling. Some airborne systems (e.g., SkyTEM) measure actual noise during production (to avoid injecting current in the transmitter every few soundings), which aids this assessment.

Our experience with AEM data affected by IP seems to show a higher apparent variability of noise. Figure 2 shows examples of such phenomena in HeliTEM transients (case study 3), showing two sets of transients with quite different noise signatures. Each set is composed of adjacent soundings, whereas the two sets were recorded 250 m apart, along the same flight line. It seems evident to us that the erratic part of the decays (usually associated with background noise) affect the two sets of transients at significantly different times and voltage levels (Figure 2a and 2b). It is also clear that these distortions show an unexpected coherence within the two sets of transients, in contradiction with the expected random behavior of background noise. Probably, the preprocessing routines (e.g., bias removal, data leveling of different types) applied by the data provider might have introduced a measurable bias onto the late part of the transient, superimposed on the random background noise. The results of manual data processing are

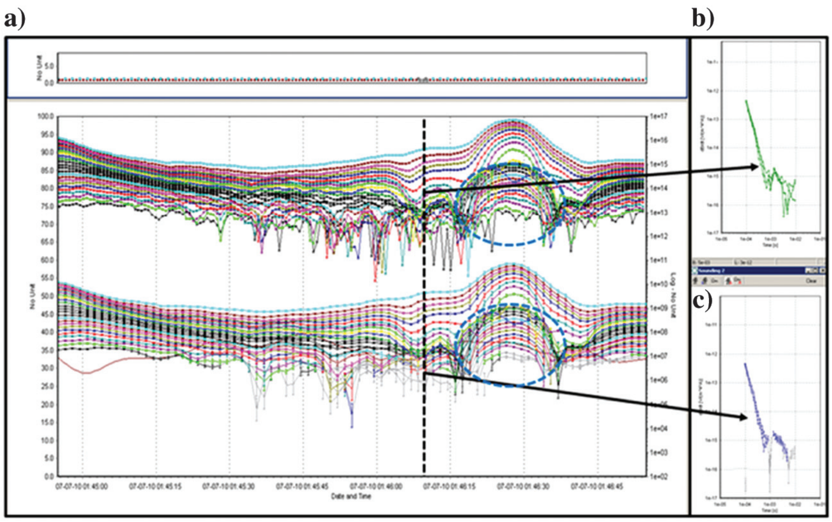

Figure 4. Example of manual data processing of VTEM data in the presence of IP effects. (a) Profile data: (top) raw and (bottom) processed. (b) Raw transients. (c) Processed transients.

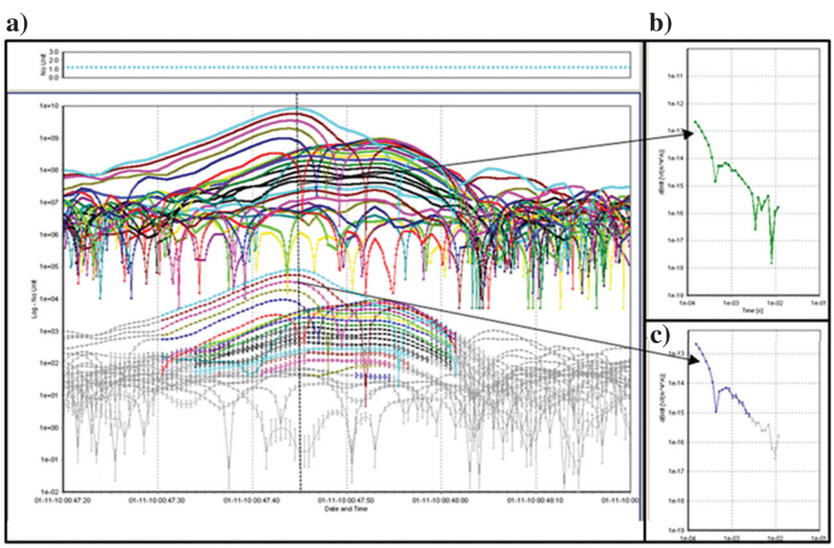

Figure 5. Example of manual data processing of HeliTEM data in the presence of IP effects. (a) Profile data: (top) raw, (bottom) processed. (b) Raw transient. (c) Processed transient.

then shown in Figure 2d–2f. The results of this processing could only be achieved in manual mode.

3) Inversion: The ultimate objective of this step of the workflow is the simultaneous multiparametric inversion of the data for the entire suite of Cole-Cole parameters using the spatially constrained inversion (SCI) algorithm (Viezzoli et al., 2008), a quasi-3D inversion code, allowing recovery of the parameters for up to 20 layers. The forward modeling kernel used in this approach is effectively 1D (Fiandaca et al., 2012), and it is capable of modeling four Cole-Cole parameters and the full transfer function of different EM systems (Viezzoli et al., 2010). The model objective function used in SCI is nevertheless 3D, by virtue of full 3D spatial coherence.
Prior to applying the simultaneous SCI to the entire data set, many individual flight lines are first inverted using the quasi-2D laterally constrained inversion (LCI) approach (Viezzoli et al., 2016). The reason for this is to account for the sensitivity of multiparametric inversion to the starting model parameters and also to counteract the ill-posedness of this inverse problem. Some dozens to hundreds of realizations are performed (Viezzoli et al., 2016), testing different combinations of the starting models parameters (for all Cole-Cole models) and regularization types (lateral constraints and variance allowed). These results are carefully assessed against ancillary geologic, geophysical, and petrophysical information that provides constraints (e.g., boreholes, geology, ground, and borehole geophysics). This assessment of the LCI results is very indicative of the quality of the data processing. Running multiple inversions often suggests ways of further refinement of the EM processing with another round of manual data editing. These LCI inversions can also suggest a reduced range of combinations to be used in the next step, the quasi-3D SCI, carried out over the entire data set (Viezzoli et al., 2008).
The standard SCI has been modified to be applied to all four Cole-Cole parameters, with each of the parameters assigned its own constraints, including upper and lower bounds and directional smoothness, which can be defined independently for each of the Cole-Cole parameters. The outcome of the SCI is balanced between the information carried by the EM data and constraints. Therefore, constraints play an important role in reducing the nonuniqueness of the output models. In Viezzoli et al. (2016), the robustness of the recovery of the different Cole-Cole models is discussed. The use of constraints and a priori information to reduce the ambiguity and extreme nonuniqueness of the inverse problem is also shown in Viezzoli et al. (2016). One of the main preliminary conclusions drawn from the synthetic studies was that it is more challenging to recover the c and τ parameters, than it is to recover ρ and m_0. However, c and τ parameters cannot be simply locked at constant values and should also be inverted for, simultaneously with ρ and m_0, because fixing them to some constant value (no matter how it is derived) can produce significant model artifacts and prevent the predicted data from fitting the observed data, or otherwise skew the distribution of chargeability to populate only the topmost part of the cross section (Viezzoli et al., 2016). The best compromise is to find the proper range and to constrain c and τ spatially within that range as tightly as possible, while fitting the data and allowing ρ and m_0 to vary. In some cases (e.g., in the presence of permafrost, lake sediments, or other well-sorted and fine-grained materials), the range of c may be based on the assumption that such materials yield higher c values (Pelton et al., 1978).

4) Data integration: Relevant ancillary information, including borehole, ground geophysical, and petrophysical data can be incorporated in the SCI (or even LCI) as an additional a priori data (Foged et al., 2014). This a priori information entered as a spatially discrete selection of borehole-derived parameters, may be further assigned spatial continuity by virtue of spatial smoothness of SCI algorithm and enforced by virtue of model objective function construction (Viezzoli et al., 2013).

5) Geologic interpretation: Given the complexity of the IP effect in AEM data and the ill-posedness of the problem, inspecting the results with a clear and critical geologic insight is a crucial part of the workflow because it helps to reduce the numerical ambiguity and select the most reasonable models. If the results are geologically unrealistic, the inversion parameters should be modified and the inversion reattempted.

RESULTS

In this section, we present the results of the modeling of AEM data affected by IP in four case studies.

Case study 1: Drybones Bay kimberlite, Northwest Territories, Canada

This case study shows results of IP inversions of VTEM data collected over Drybones kimberlite in Northwest Territories, Canada (Figure 6). This kimberlite lies completely underneath the waters of Drybones Bay (Great Slave Lake) at an average depth of 38 m (Kerr et al., 2001). There is a significant cover of clays and till sediments present, overlaying the consolidated kimberlite. Cross section AA′ in Figure 6 was drawn across the Drybones kimberlite, based on drilling information.

Morphologically, the kimberlite is a spatially elongated intrusion (900×400 m), consisting of crater pyroclastic and diatreme facies (Kretschmar, 1995). The host geology in the Drybones area consists of resistive igneous rocks. Metasediments of the Yellowknife Supergroup are also present (Dunn et al., 2001). In addition, there are several known tectonic faults present in the direct vicinity of the kimberlite area and a diabase dike in the northern part crosses the area from east to west.

There were two airborne surveys flown over the kimberlite: a VTEM TDEM survey in 2005 and a Z-axis time domain electromagnetic (ZTEM) natural field EM survey in 2009 (Kaminski et al., 2010). Some portions of the ZTEM flight lines coincide with the VTEM flight lines. VTEM data display a moderate to strong IP effect. These data were previously modeled and inverted without application of Cole-Cole modeling using 3D-TDEM and 3D-ZTEM inversion algorithms (Kaminski and Oldenburg, 2012). In this study, the VTEM data were reprocessed and reinverted using the multiparametric SCI approach. The starting model parameters and constraints used in the inversion are shown in Table 1. The inversion allowed recovery of improved electrical resistivity and chargeability distributions. The results of SCI inversion with Cole-Cole modeling are shown in Figure 7 as a cross section of resistivities over VTEM line 70 (which is coincident with a part of ZTEM line 1210).

The results of SCI inversion with Cole-Cole modeling were verified against drilling information. Figure 8 shows interpolated depth slices of electrical resistivity and chargeability for the depth interval 100–120 m, which corresponds to the upper (weathered) part of the Drybones kimberlite. As shown in Figure 8, the upper part of the kimberlite is imaged as moderately conductive and moderately chargeable, which is consistent with results of Viezzoli and Kaminski (2016) acquired over Amakinsaya kimberlite pipe (Russia). These results suggest that recovering chargeability values from this depth using airborne TDEM data inversion with IP modeling appears feasible, although the recovered values are on the limits of predicted sensitivity (depth of investigation).

Finally, Figure 9 presents results of multiparametric SCI inversion, interpolated along the profile AA′ shown earlier in Figure 6. The results have been matched with the results of 3D VTEM inversion (Figure 9a) presented in Kaminski and Oldenburg (2012). There are obvious mismatches in the top portion of the cross section. It is shown in the figure that Kaminski and Oldenburg (2012) suggest that the electrical conductivity of lake waters is similar to the electrical conductivity of clay and till sediments, whereas the SCI inversion with IP modeling (Figure 9b) is suggesting that the clay sediments are more conductive than the lake waters. The latter is more geologically realistic in our view and also in better agreement with the ZTEM inversion results (Figure 7), with understanding that the ZTEM system is not affected by IP at the frequencies corresponding to the VTEM bandwidth (Gasperikova et al., 2005). The recovered chargeability is shown in Figure 9c and matches very well with the lake sediments. It is expected that the lake sediments form the most chargeable rock type in this cross section due to high volume of clay material present.

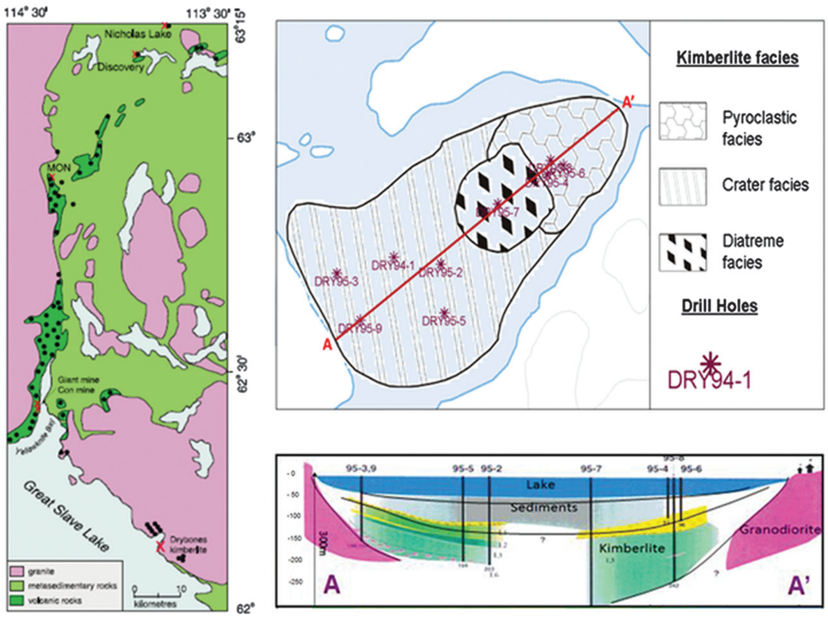

Figure 6. Location of Drybones kimberlite in NWT, Canada; lithologic cross section along the AA′ profile (adapted from Kerr et al., 2001).

Table 1. Starting models (half-space) and types of constraints used in the SCI inversions of field data.

	ρ	m_0	τ	c
Case study 1	300	100	1.00E-03	0.5
Case study 2	100	50	1.00E-04	0.3
Case study 3	1000	60	1.00E-04	0.5
Case study 4	100	50	1.00E-03	0.6
		Vertical constraints		
Case study 1	Soft	Moderate	Hard	Very hard
Case study 2	Soft	Moderate	Hard	Hard
Case study 3	Soft	Soft	Hard	Hard
Case study 4	Soft	Moderate	Very hard	Very hard
		Horizontal constraints		
Case study 1	Soft	Soft	Moderate	Moderate
Case study 2	Soft	Soft	Hard	Hard
Case study 3	Soft	Soft	Moderate	Moderate
Case study 4	Soft	Moderate	Very hard	Very hard

Case study 2: VMS exploration, Oman

This case study is, in our view, especially interesting from two standpoints: the way it originated and because the featured IP anomaly was not immediately apparent. The survey was flown in 2012 over a part of the Arabian Peninsula using the VTEM system. The survey was aimed at volcanogenic massive sulphide (VMS) targets, characterized by high electrical conductivity. Several data analysis and modeling techniques were used in the initial stage of interpretation, including Maxwell plate modeling, 2D resistivity depth imaging (Meju, 1998), and exponential decay time-constant analysis (Nabighian and Macnae, 1991).

The potential for IP effects being present in the VTEM data set was not considered and was not directly evident. The preliminary data interpretation carried out by the geophysical contractor was successful in identifying several targets. Plate modeling and resistivity depth images were used at this stage, which were later confirmed by drilling.

Although these techniques proved effective on some targets, they nonetheless have missed at least one known occurrence, which was smaller in size and was hosting copper mineralization (Figure 10a). New attempts to image this occurrence in the model space were carried out using different techniques, including an SCI inversion without consideration of the IP effect, as well as a multilayered inversion routine (Vignoli et al., 2013). This initial work did not consider the IP effects. The obtained SCI models revealed some uncertain indications of a conductive target (Figure 10c), which had been previously unseen in the initial interpretation phase, neither in 2D conductivity-depth transforms nor in time-constant analysis (Figure 10d). Furthermore, as shown, the data fit over the occurrence was poor and the conductor was imaged close to the surface and in contradiction with the drilling information, which intersected the massive sulfide at greater depth (Figure 10c).

This case was revisited at a later time, after the presence of a subtle IP effect was suspected in the data. Lengthy research was conducted during 2015–2016 (Kaminski et al., 2015, Viezzoli et al., 2015b, 2015a, 2016), which included studies at many different locations from around the world with the IP effect present. Closer inspection revealed IP-like features affecting the early times and showing increased voltages in transients, as well as middle-time gate measurements subject to subtle signal suppression (Figure 10b). No negative voltages were observed. The data were therefore reprocessed manually (e.g., step 2 in the "Methodology" section) and inverted using a 20-layer Cole-Cole model. The starting model parameters and constraints used in the SCI inversion are shown in Table 1. The results provided a significantly improved target recovery: A deeper chargeable target was predicted and in better general agreement with the drilling information acquired over the known mineralization (Figure 11). As shown in Figure 11, the parameters τ and c were allowed to vary because it is very challenging to achieve satisfactory data fit with having them fixed (Viezzoli et al., 2016). The data fit was significantly improved compared with the "no-IP" inversion attempts. It seems unlikely that this is the only such case when the IP effects are masking bedrock conductors.

Case study 3: Natashquan Ni-Cu-PGE Project, Labrador, Canada

This case study illustrates the interpretation of a chargeable body at significant (100 m) depth that has been confirmed by drilling and laboratory measurements performed on the drill core. The airborne TDEM survey was flown using the HeliTEM system in 2013 over Altius Resources Inc.'s Natashquan nickel-copper-platinum group elements (PGE) Project in Labrador, Canada, which contains some extreme, localized IP effects (Kaminski et al., 2015). In some parts, the survey showed entirely negative transients (Figures 1e and 5). These data were therefore unsuited for conventional TDEM resistivity inversions approach, unless Cole-Cole modeling was implemented. Figures 12 and 13 show the results of SCI inversion as 2D slices and in profile. The starting model parameters and constraints used in the inversion are shown in Table 1.

The data misfits were very low, showing good convergence to target misfit, measured as the difference between the observed and predicted data, normalized by standard deviation (Figure 13). A conductive and chargeable body was predicted to a depth of 100 m beneath the shallow lake. The isovolumes of conductivity and chargeability were used by the interpreter to design an oblique drillhole to intercept the predicted target. The presence of the target was confirmed by drilling, and then the recovered drill core was subjected to direct measurements of conductivity and chargeability using the time domain induced polarization (TDIP) portable system (GDD instrumentation).

The direct-core measurements (Figure 13 and Table 2) show a general correlation with the values predicted by the multiparametric inversions of HeliTEM data, notwithstanding the fact that the ranges of resistivities and chargeabilities need to be scaled for better agreement, subject to instrumentation considerations. Laboratory tests fully confirm the presence of the deep chargeable and conductive target at the predicted depth, overlain by locally resistive and less chargeable strata. Given the different methodologies of chargeability measures obtained from AEM and from direct sampling of the core, one should not expect identical absolute values. The TDIP core measurements were carried out at a 0.5 Hz base frequency, whereas the operating base frequency of the HeliTEM system is 30 Hz. Nonetheless, in this case, the AEM data inversion and the direct-core measurements recovered values on the order of hundreds of millivolts per volt for the chargeability maximum. The conductor imaged through inversion and intercepted by the drilling did not display the anticipated increased voltage response in the data space, before accounting for the IP effect.

Case study 4: Jervois copper deposit, Australia

In this example, a VTEM survey was flown in the Northern Territories, Australia (Figure 14), over an area in the Jervois domain,

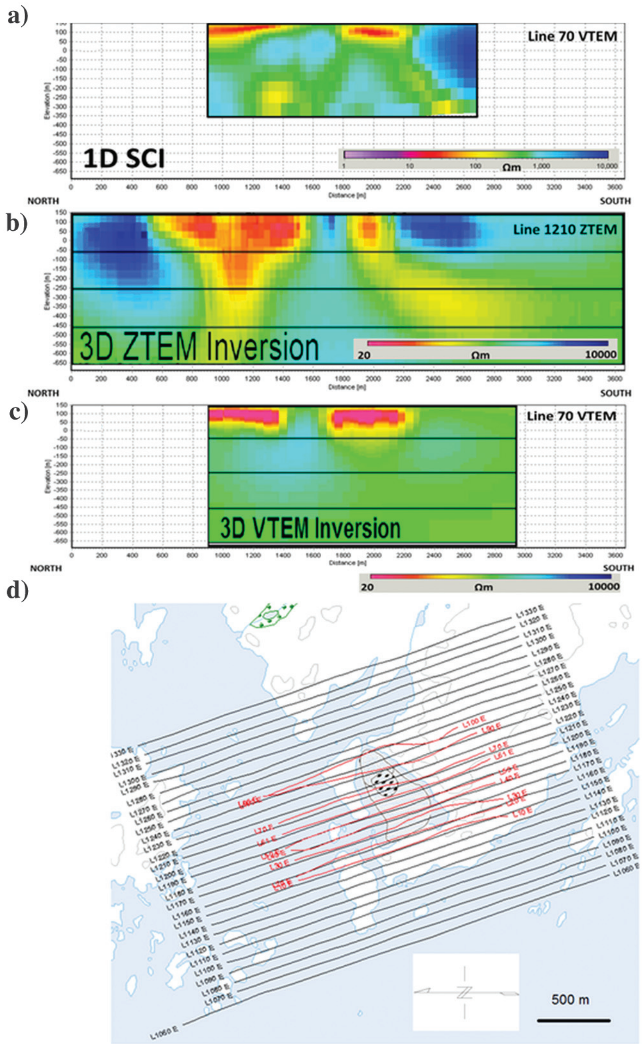

Figure 7. (a) Results of SCI inversion with Cole-Cole modeling. (b) Results of 3D ZTEM inversion (adapted from Kaminski and Oldenburg, 2012). (c) Results of 3D TDEM inversion (adapted from Kaminski and Oldenburg, 2012). (d) VTEM (red)/ZTEM (black) flight planning over Drybones kimberlite.

which is prospective for Beshi-type Sedex/VHMS deposits. All areas shown in this figure are subject to ongoing exploration activities; however, we will discuss only those areas crossed by reference profile FF′. The collected airborne data have strong evidence of the IP effect. In this case, the IP effects display distinct and clear features over different outcropping geologies. Figure 3 presents the dB/dt profile from a single flight line of this survey with interpreted IP effects due to three different rock types (alluvium, schist, and granite).

The aim of the VTEM survey was to detect buried bedrock conductive targets related to potential deposits. The presence of IP effects in AEM data also allowed the recovery of bedrock chargeable targets. This was achieved through modeling of Cole-Cole parameters in the multiparametric SCI inversion, thereby obtaining the 3D distributions of ρ and m_0, and imaging them at depth below the overburden. The starting model parameters and constraints used in the SCI inversion are shown in Table 1. This was the largest and the most computationally expensive case study out of the four described in this paper, involving the simultaneous inversion of more than 14,000 stations, carried out in approximately 24 h.

As indicated in earlier examples, it is important to invert for c and τ parameters, while at the same time limiting their variance within certain ranges using "soft" constraints (Viezzoli et al., 2016). After manual data processing and assessment of preliminary multiparametric LCI inversions (see step 3 of the workflow for details), it became evident that there was a series of domains within which c and τ parameters were relatively homogenous, but between these domains, the c and τ parameters varied more abruptly. The preliminary LCI inversions also showed that the optimal starting models were not homogeneous across the entire survey. For these reasons, the multiparametric SCI inversion was setup with a special focus on such areas. Different starting models, as well as regularization constraints and varying smoothness were used in the SCI inversion. The inversion results showed good data fit (Figure 15). The interpolated results over section "F" (Figure 14) were further matched with drilling information (Figure 16). For comparison, there was a "non-IP" inversion, carried over the same area. The results of the non-IP inversion, interpolated over section F, are shown in Figure 17. As is evident from the resistivity depth sections in Figures 16 and 17, the inversion without Cole-Cole modeling poorly maps the known thickness of the overburden, compared with multiparametric inversion.

The resistivity derived from the SCI inversion was used to generate an isosurface using a 10 ohm-m threshold. This isosurface was further interpreted as the bottom of the conductive overburden (regolith). Some of the final results of the multiparametric SCI inversion are presented in Figure 18. From Figure 18a to 18d, it can be observed how rapidly the electrical and chargeable properties vary in the vertical direction. In addition, these results display a large spatial variability in ρ and m_0. As mentioned earlier, the frequency parameter c varies abruptly across the major domains, while remaining rather constant within them (Figure 18e). The map of the thickness of chargeable material below the superficial conductor (overburden) provides an interesting proxy of basement targets recommended for follow-up using ground geophysical surveys and other methods (Figure 18f). In general, most other transients, including those with substantial negative voltages, are well-fit (e.g., Figure 15).

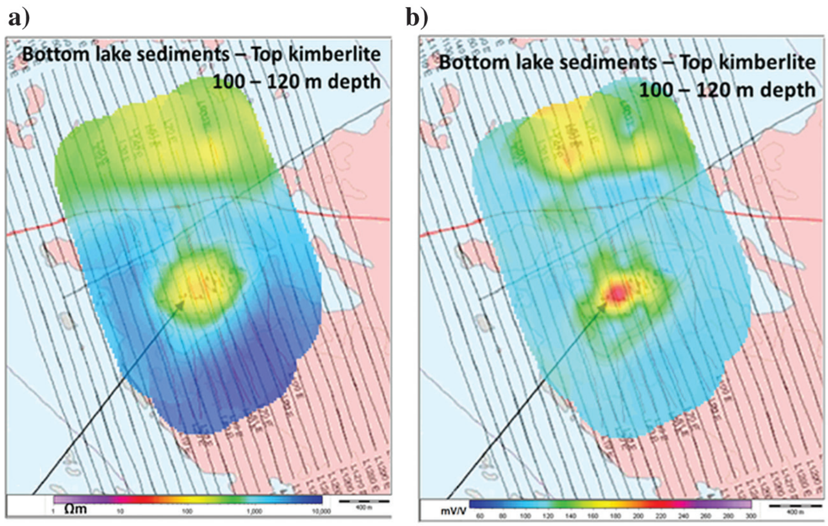

Figure 8. Interpolated results of SCI Cole-Cole inversion. (a) Resistivity at depth interval 100–120 m below surface. (b) Chargeability at a depth interval of 100–120 m below surface.

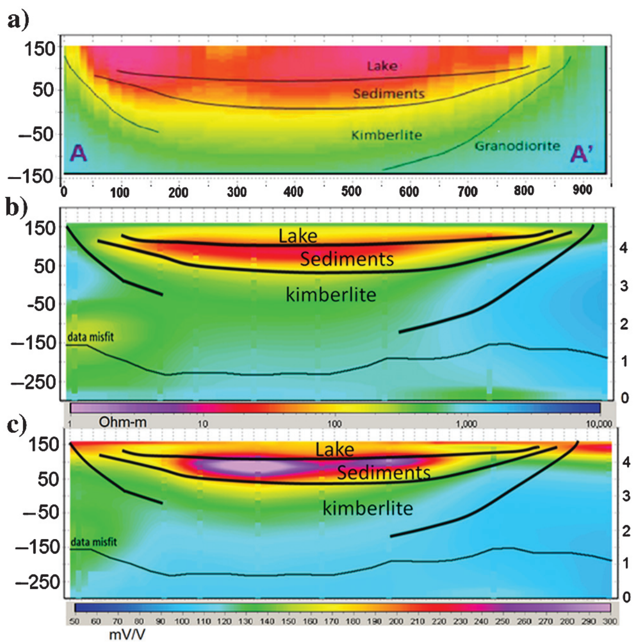

Figure 9. (a) Electrical resistivity recovered from 3D TDEM inversion (adapted from Kaminski and Oldenburg, 2012). (b) Interpolated resistivity cross section along profile AA′. (c) Interpolated chargeability cross section along profile AA′.

DISCUSSION

From a methodological viewpoint, it is very encouraging that the procedures and techniques applied (even though based on 1D forward responses) appeared to produce credible results that were also confirmed by ground truth. The scenarios were very diverse in terms

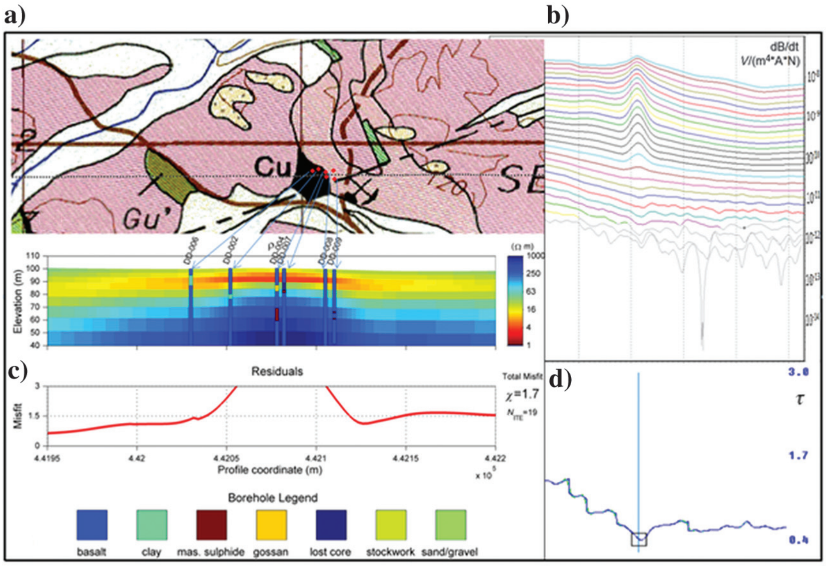

Figure 10. (a) Location of known occurrence (Cu) over a geologic map. (b) The occurrence as seen in VTEM data. (c) Results of no-IP inversion with usage of advanced processing techniques. (d) Calculated time constant.

of the geology, targets, TDEM systems, type and intensity of IP effects in the data space, as well as source and geometry of the chargeable anomalies in the model space. In each case, the IP modeling contributed toward a better understanding of the subsurface.

- First, the improvements in the resistivity models should not be underestimated. Better resistivity models produce better geologic models, easier integration, and comparison with ancillary information (which is typically available).
- Second, the extraction of another, very useful, physical property chargeability from the existing data adds obvious value to exploration. The extraction of c and τ parameters, although not thoroughly discussed in this paper, should contribute to geologic mapping in the future.
- Third, the capability of keeping all observed field data and using it in the inversion — as opposed to disregarding those data affected by IP, which historically has been a standard practice in the industry — adds more usable data and hence potentially adds to more useful information obtained from the TDEM surveys.

The widely varying manifestations of IP effects in TDEM data require the application of careful manual data processing. As discussed in detail in Viezzoli et al. (2016), the ill posedness of the multiparametric inversion requires that several test inversions be attempted before settling on the most appropriate starting model parameters and regularization types. For example, our experience shows the need to mindfully allow some variance in the c and τ parameters to obtain a proper data fit. The input of a priori ancillary information (i.e., from boreholes, surface geophysics, or geologic

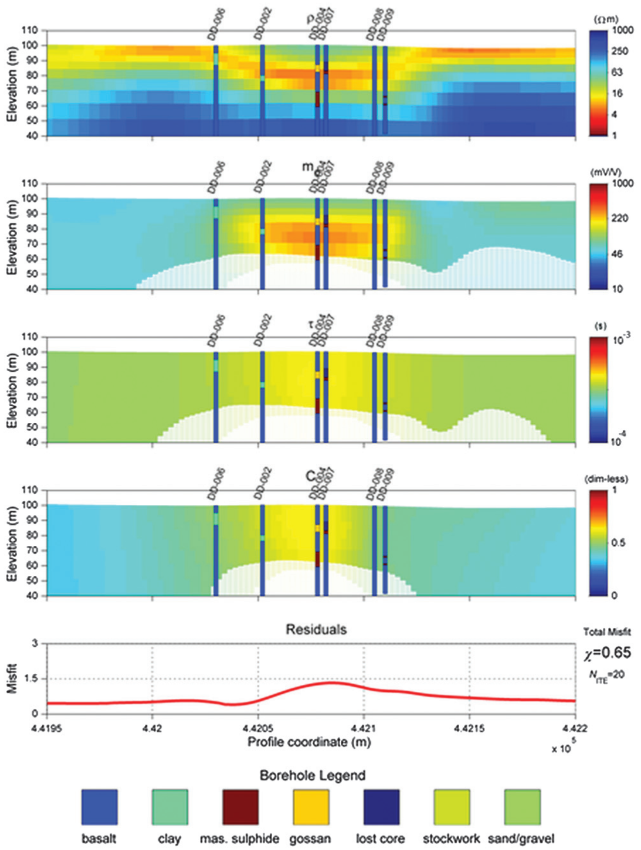

Figure 11. Inversion of VTEM data in IP-mode with recovery of four Cole-Cole parameters, from top to bottom: electrical resistivity ρ, chargeability m_0, time constant τ, and frequency parameter c.

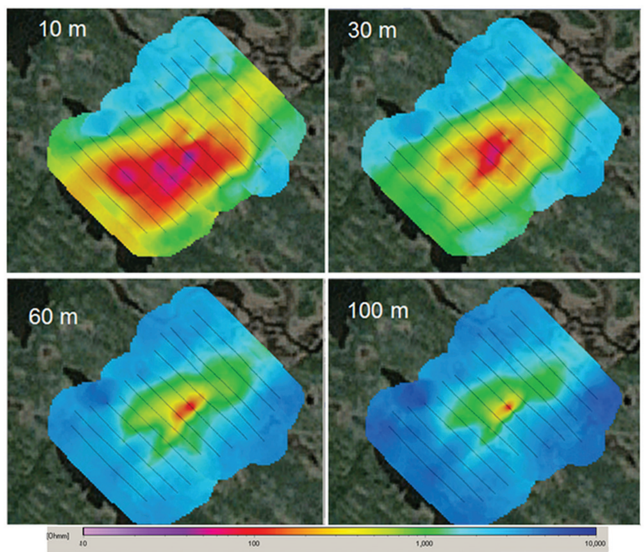

Figure 12. Gridded electrical resistivity slices recovered by SCI IP-mode inversion, shown at different depths below the surface.

models) into the inversion may also be highly beneficial. Analyzing the inversion results with geologic insight is also of the utmost importance.

It is also worth mentioning, that having the capability of modeling IP effects allows flexible testing of different model scenarios. For example, the presence of a deeply buried conductor manifested mainly in late time transients, may be partially or fully masked by IP effects from shallower geology (Viezzoli et al., 2016). In such case, the standard approach to fitting an exponential (τ analysis) at late times would also miss the deep conductor, as shown in case study 2. Furthermore, the simultaneous inversion for all Cole-Cole model parameters aims at estimating their actual distribution in the subsurface, as opposed to other sequential approaches that yield apparent values.

Our experience suggests that a substantial portion of helicopter TDEM surveys flown with AEM systems of good signal-to-noise ratio (S/N) can be sensitive to IP effects, especially those surveys flown in permafrost environments and in the presence of clay alterations and disseminated mineralizations. This obviously holds for targets such as kimberlites and sulfides, but it can also be attributed to other sources. Among other examples, weathered, iron-rich overburden (Australia, parts of Africa) and permafrost (Canada, Russia) can produce measurable IP effects. In some cases, these coexist with exploration targets. The potential presence of IP signatures in AEM data does not apply only to the new data, but also to existing data. It is likely that data acquired with powerful systems (continuously developed and improved from the early 2000s) could contain some IP signatures that could probably be recovered. It also means that the same data, in case it had been modeled without IP, might have produced systematically inaccurate resistivity models that could be rectified.

In these two papers (the present and Viezzoli et al., 2016), we focus on helicopter EM systems because they show the most evident IP effects suitable for modeling due to the lower flight altitude and higher S/N, when compared with fixed-wing equivalents. However, the fixed-wing systems are also sensitive to IP (Smith and Klein, 1996). As a matter of fact, there is ongoing research (Macnae, 2015b) that this type of geometry is preferable to produce higher IP responses, although not inductive but galvanic, and generated by deeper seated targets. On the other hand, the higher degrees of free-

Table 2. Results of electrical measurements over the core from a drill aimed at the conductive and chargeable anomaly as recovered from AEM data in case study 2.

Position (m) along the drilling path (45° dip angle)	Resistivity (Ωm)	Chargeability (mV/V)
24	4024.4	5.100
60	5314.4	1.600
83	7369.9	10.6
93	781.5	1.4
109	3187.5	4.0
141	3673.9	4.4
155	19.0	116.1
167	9.2	241.5
181	7.6	231.6
201	173.0	3.5

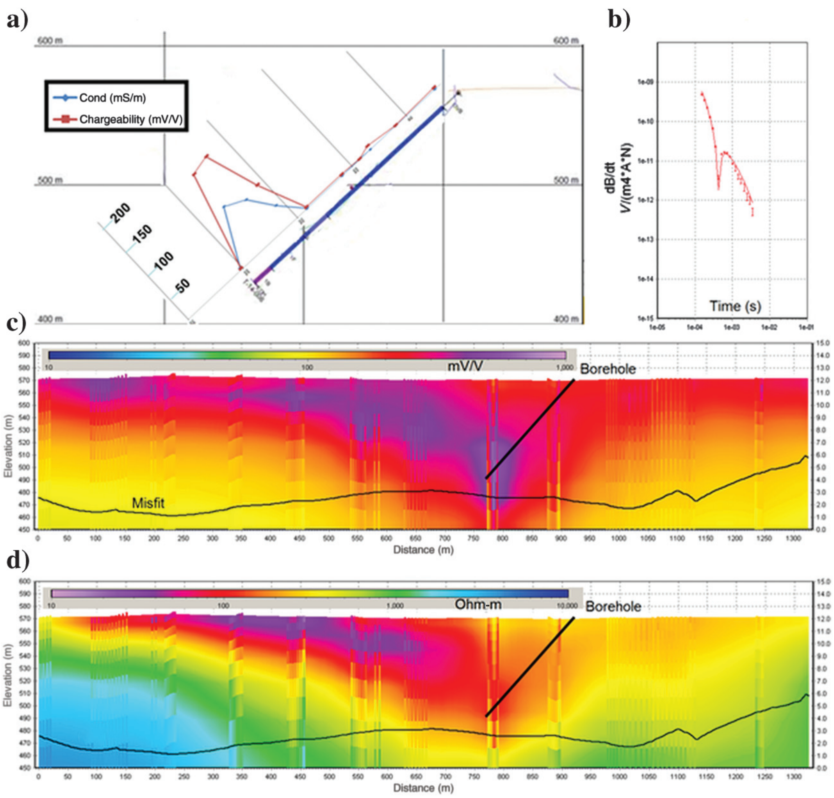

Figure 13. Results of SCI inversion shown as a cross section, interpolated across the flight lines and over the target, showing the location of the drillhole and physical property measurements (see Table 1 for details). (a) TDIP core physical property measurements. (b) Observed data versus predicted data in a single transient (data fit). (c) Interpolated chargeability section. (d) Interpolated electrical resistivity section.

dom associated with the varying Tx-Rx relative positions and orientation (rarely recorded properly) may increase the nonuniqueness of the problem to a greater degree. More research and experimental evidence is needed with fixed-wing systems to assess their actual usefulness for recovering accurate chargeability models.

The last point of this discussion revolves around the limitations of using a layered earth 1D response, as it is shown in our studies, for IP modeling of helicopter TEM data. The argument that the subsurface is 3D and not 1D is conceded. On the other hand, there are three major advantages in favor of using the 1D approach:

- First, 1D models are appropriate in some geologies, especially in those, which can be well-described by a layered earth approximation.
- Second, full 3D inversions are computationally very expensive. Even though this no longer means that only small surveys can be inverted (Cox et al., 2010), it still imposes limitations on the number of inversions applicable for practical usage and to fine tune the starting model parameter selection.
- Third, the 3D approach may represent a serious impediment because the number of time gates used for modeling is often

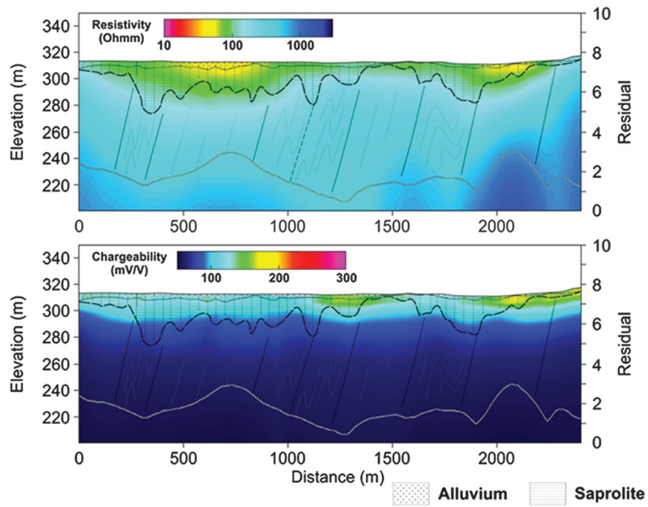

Figure 16. Results of SCI inversion in IP-mode (electrical resistivity and chargeability), interpolated over section F (Figure 14) with the depth to bedrock (thick dashed line) drawn based on drilling information. Residual is shown as thin gray line at the bottom, scaled to the right vertical axis.

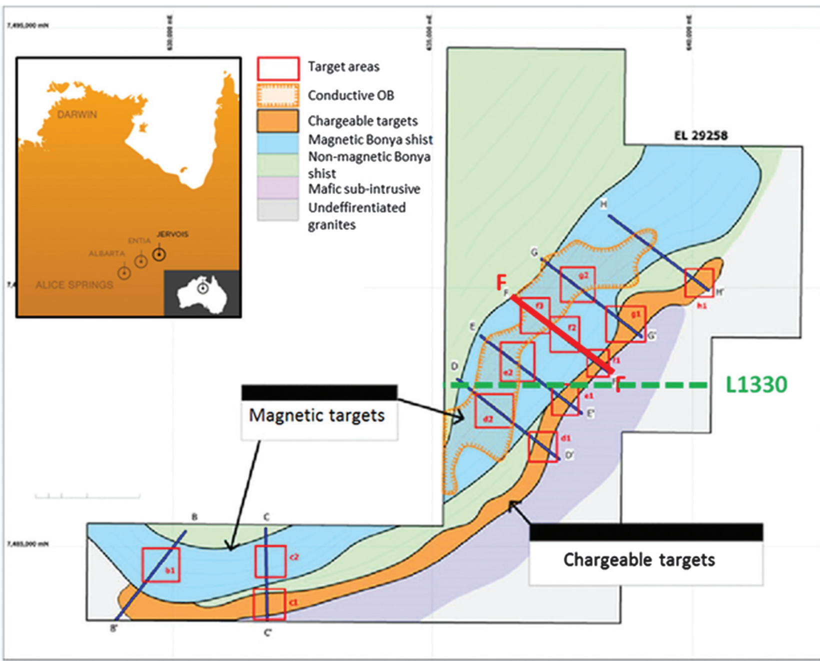

Figure 14. Location of Jervois copper project, Northern Territories (Australia).

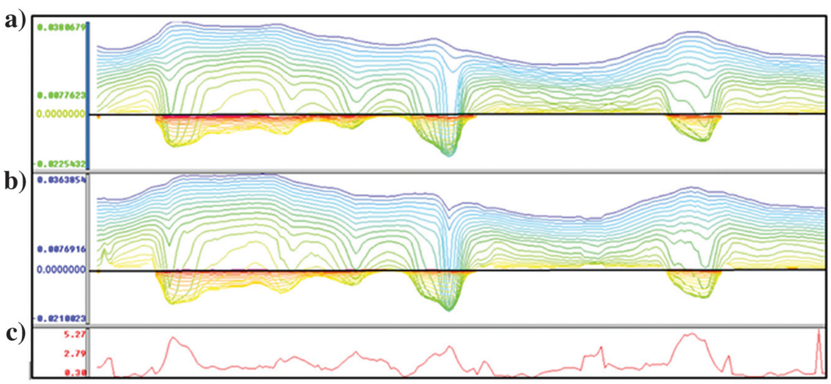

Figure 15. Data fit of the SCI inversion, shown for flight line 1330. (a) Observed VTEM data. (b) Predicted VTEM data. (c) SCI misfit, normalized by standard deviation.

reduced with respect to the measured full transient (Yang and Oldenburg, 2012). Increasing the dimensionality to three dimensions may also bring along an even higher degree of nonuniqueness, which can be detrimental in the already very ill-posed multiparametric IP inverse problem.

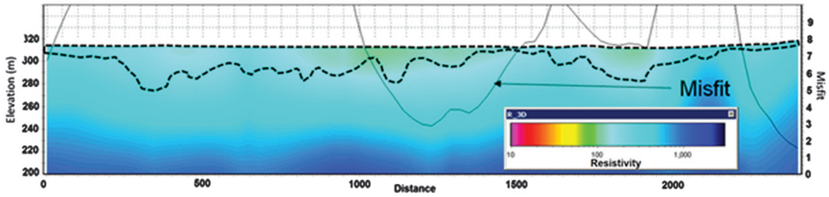

Figure 17. Results of SCI inversion in non-IP mode (electrical resistivity) interpolated over section F (Figure 14) with the depth to bedrock drawn based on drilling information (see Figure 16 for details).

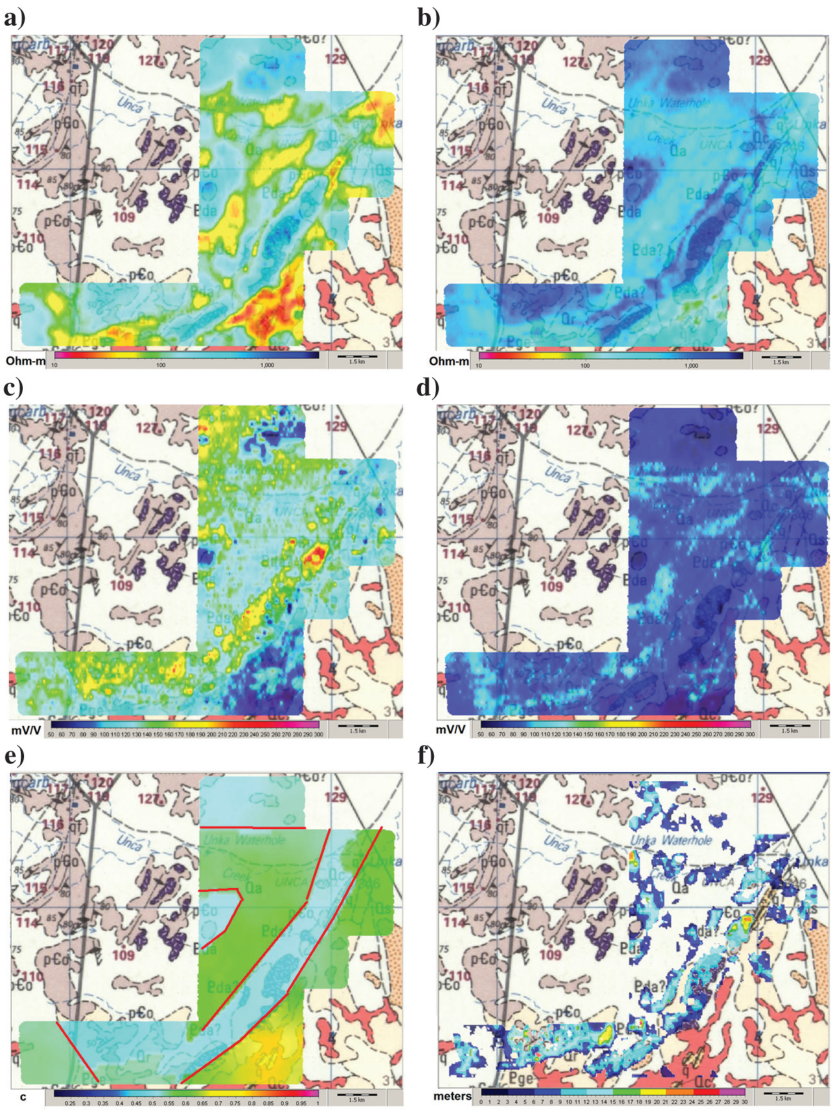

Figure 18. Results of SCI Cole-Cole inversion over a copper prospect in Northern Territories, Australia. (a) Recovered electrical resistivity at 10–20 m interval. (b) Recovered electrical resistivity at 80–100 m interval. (c) Recovered chargeability at 0–10 m interval. (d) Recovered chargeability at 20–30 m interval. (e) Recovered frequency parameter c at 0–10 m interval. (f) Thickness of chargeable material below the interpreted thickness of the conductive overburden.

From the commercial standpoint of providing fast and reliable inversion of large-scale data sets, even when the full 3D inversions become sufficiently fast to overcome any computational limitations, the 1D solution will still represent a robust and useful approach. The 3D code may therefore be used in parallel with one dimension (on deposit scale for example), and should be seen as a tributary, rather than an alternative.

CONCLUSION

IP effects can manifest themselves in TDEM data in different ways, from more to less obvious, and they can vary remarkably over relatively short distances. This, together with the ill-posed multiparametric inversion problem, calls for a customized workflow to be made consisting of careful manual data processing, extensive preparatory modeling, and critical analysis of results.

The case studies presented here illustrate that this holistic workflow (based on 1D forward responses) can be successfully applied to different exploration targets, from kimberlites (case study 1) to VMS and other base metal targets. Failure to account for IP effects, when present, produces erroneous resistivity models (as shown in case studies 2 and 4). On the other hand, modeling IP allows extraction of corrected resistivity models, as well as realistic volumetric models of chargeability, which may be associated with valid exploration targets. Recoverable IP signatures in TDEM data are not limited to near-surface sources, but can originate from targets in excess of 100 m of depth (case study 3). The exploration and geologic modeling might benefit significantly from reprocessing and modeling of historic TDEM data sets using the suggested Cole-Cole models. It is possible that, similar to case study 2, exploration targets missed in the original standard processing may be recovered when reprocessed. It is also possible that widespread, perhaps unrecognized, IP effects from weathered overburden or permafrost might have introduced artifacts in previous interpretations that could potentially mask deeper conductors related to mineral deposits.

ACKNOWLEDGMENTS

We would like to thank Geotech, Ltd., for providing the VTEM data, collected over the Drybones kimberlite for research purposes; Core Exploration, Ltd., for allowing the publication of Jervois VTEM data; Altius Resources Inc. and Anglo American Exploration Canada Ltd.; and Mawarid Mining, T. Munday, and Y. L. Cooper of CSIRO for their input into interpretation of the Jervois VTEM data; and D. Di Massa for his input in inversion and interpretation of the Drybones kimberlite VTEM data.

REFERENCES

Auken, E., A. V. Christiansen, J. Westergaard, C. Kirkegaard, N. Foged, and A. Viezzoli, 2009, An integrated processing scheme for high-resolution airborne electromagnetic surveys, the SkyTEM system: Exploration Geophysics, **40**, 184–192, doi: 10.1071/EG08128.

Chen, T., G. Hodges, and A. Smiarowski, 2015, Extracting subtle IP responses from airborne time domain electromagnetic data: 85th Annual International Meeting, SEG, Expanded Abstracts, 2061–2066.

Cole, K. S., and R. H. Cole, 1942, Dispersion and absorption in dielectrics: Journal of Chemical Physics, **9**, 341–351, doi: 10.1063/1.1750906.

Cox, L. H., G. A. Wilson, and M. S. Zhdanov, 2010, 3D inversion of airborne electromagnetic data using a moving footprint: Exploration Geophysics, **41**, 250–259, doi: 10.1071/EG10003.

Dunn, C. E., D. Smith, and D. E. Kerr, 2001, Biogeochemical survey of the Drybones Bay area, NWT using outer bark of black spruce: Geological Survey of Canada, Open File 3919.

Gasperikova, E., N. H. Cuevas, and H. F. Morrison, 2005, Natural field induced polarization for mapping of deep mineral deposits: An example from Arizona: Geophysics, **70**, no. 6, B61–B66, doi: 10.1190/1.2122410.

Fiandaca, G., E. Auken, A. V. Christiansen, and A. Gazoty, 2012, Time-domain-induced polarization: Full-decay forward modeling and 1D laterally constrained inversion of Cole-Cole parameters: Geophysics, **77**, no. 3, E213–E225, doi: 10.1190/geo2011-0217.1.

Foged, N., P. A. Marker, A. V. Christiansen, P. Bauer-Gottwein, F. Jørgensen, A.-S. Høyer, and E. Auken, 2014, Large scale 3D-modeling by integration of resistivity models and borehole data through inversion: Hydrology and Earth System Sciences, **18**, 4349–4362, doi: 10.5194/hess-18-4349-2014.

Flis, M., G. A. Newman, and G. W. Hohmann, 1989, Induced polarization effects in time domain electromagnetic measurements: Geophysics, **54**, 514–523, doi: 10.1190/1.1442678.

Lane, R., A. Green, C. Colding, M. Owers, P. Pik, C. Plunkett, D. Sattel, and B. Throne, 2000, An example of 3D conductivity mapping using the TEMPEST airborne electromagnetic system: Exploration Geophysics, **31**, 162–172, doi: 10.1071/EG00162.

Kamenetsky, F., G. Trigubovich, and A. Chernyshev, 2014, Three lectures on geological medium induced polarization: Ludwig-Maximilian University of Munich.

Kaminski, V., J. Legault, and H. Kumar, 2010, The Drybones kimberlite: A case study of VTEM and ZTEM airborne EM results: 21st International Geophysical Conference and Exhibition, ASEG, Expanded Abstracts, 1–4.

Kaminski, V., and D. W. Oldenburg, 2012, The geophysical study of Drybones Kimberlite using 3D TDEM inversion and 3D ZTEM inversion algorithms: 22nd International Geophysical Conference and Exhibition, ASEG, Expanded Abstracts, 1–4.

Kaminski, V., A. Viezzoli, A. Menghini, and G. Fiandaca, 2015, Case studies of modeling IP effect in AEM data: 21st European Meeting of Environmental and Engineering Geophysics, EAGE, Extended Abstracts.

Kerr, D. E., R. D. Knight, D. Smith, and D. Nickerson, 2001, Drift prospecting investigations in the Yellowknife Greenstone belt, NWT: National Resources Canada.

Kretschmar, U., 1995, Drill report on the Drybones Bay Kimberlite property, Drybones Bay, Great Slave Lake, District of MacKenzie, Northwest Territories, Canada: Technical Report, NWT Department Indian & Northern Affairs Mining Recorder.

Kwan, K., J. Legault, A. Prikhodko, and E. Goncharov, 2015, Airborne inductively induced polarization effects in and their removal from the VTEM data from Mirny, Russia: 85th Annual International Meeting, SEG, Expanded Abstracts, 2032–2036.

Macnae, J., 2015a, Quantifying airborne induced polarization effects in helicopter time domain electromagnetic: Journal of Applied Geophysics, published online, doi: 10.1016/j.jappgeo.2015.10.016.

Macnae, J., 2015b, Airborne IP: Can it be more than scratch of a surface: Presented at the South African Geophysical Association Annual Meeting and Conference, Workshop on modeling IP.

Macnae, J.., 2015c, Comment on Tarasov, A., and K. Titov, 2013, On the use of Cole-Cole equations in spectral induced polarization: Geophysical Journal International, **195**, 352–356.

Macnae, J., Y. Lamontagne, and G. West, 1984, Noise processing techniques for time domain EM systems: Geophysics, **49**, 934–948, doi: 10.1190/1.1441739.

Meju, M., 1998, A simple method of transient electromagnetic data analysis: Geophysics, **63**, 405–410, doi: 10.1190/1.1444340.

Nabighian, M., and J. Macnae, 1991, Time domain electromagnetic prospecting methods, *in* E. B. Neitzel, ed., Electromagnetic methods in applied geophysics — Part A: Applications: SEG Investigations in Geophysics 3, 427–509.

Pelton, S. H., S. H. Ward, P. G. Hallof, W. R. Sill, and P. H. Nelson, 1978, Mineral discrimination and removal of inductive coupling with multifrequency IP: Geophysics, **43**, 588–609, doi: 10.1190/1.1440839.

Prikhodko, A., E. Morrison, A. Bagrianski, P. Kuzmin, P. Tischin, and J. Legault, 2010, Evolution of VTEM: Technical solutions for effective exploration: 21st International Geophysical Conference and Exhibition, ASEG, Expanded Abstracts, 1–4.

Smith, R. S., 1989, Induced polarization effects in time domain electromagnetic measurements: Geophysics, **54**, 514–523, doi: 10.1190/1.1442678.

Smith, R. S., and J. Klein, 1996, A special circumstance of airborne induced polarization measurements: Geophysics, **61**, 66–73.

Smith, R. S., and G. F. West, 1988, Inductive interaction between polarizable conductors: An explanation of a negative coincident-loop transient electromagnetic response: Geophysics, **53**, 677–690, doi: 10.1190/1.1442502.

Tarasov, A., and K. Titov, 2013, On the use of Cole-Cole equations in spectral induced polarization: Geophysical Journal International, **195**, 352–356, doi: 10.1093/gji/ggt251.

Vignoli, G., G. Fiandaca, A. V. Christiansen, C. C. Kirkegaard, and E. Auken, 2013, Sharp spatially constrained inversion: 19th European Meeting of Environmental and Engineering Geophysics, Expanded Abstracts, 1–4.

Viezzoli, A., A. V. Christiansen, and E. Auken, 2010, Increased accuracy for quantitative modeling of airborne EM data through detailed description of system transfer function and spatially constrained inversion: 21st International Geophysical Conference and Exhibition, ASEG, Expanded Abstracts, 1–3.

Viezzoli, A., A. V. Christiansen, E. Auken, and K. Sorensen, 2008, Quasi-3D modeling of airborne TEM data by spatially constrained inversion: Geophysics, **73**, no. 3, F105–F113, doi: 10.1190/1.2895521.

Viezzoli, A., G. Fiandaca, S. Segio, and E. Auken, 2013, Constrained inversion of IP parameters from Airborne EM data: 23rd International Geophysical Conference and Exhibition, ASEG, Expanded Abstracts, 1–4.

Viezzoli, A., F. Jorgensen, and C. Sorensen, 2012, Flawed processing of airborne EM data affecting hydrogeological interpretation: Groundwater, **51**, 191–202.

Viezzoli, A., and V. Kaminski, 2016, Airborne IP: Examples from Mt. Milligan deposit, Canada and Amakinskaya kimberlite pipe, Russia: Exploration Geophysics, doi: 10.1071/EG16015.

Viezzoli, A., V. Kaminski, and G. Fiandaca, 2016, Modeling induced polarization effects in helicopter time domain electromagnetic data: Synthetic case studies: Geophysics, **82**, this issue, doi: 10.1190/geo2016-0096.1.

Viezzoli, A., V. Kaminski, and E. M. Goncharov, 2015a, Airborne IP, examples from gold and kimberlite exploration: 7th International AEM Conference and Exhibition, SAGA, Expanded Abstracts.

Viezzoli, A., V. Kaminski, Y. Ley-Cooper, L. Hardy, and G. Fiandaca, 2015b, Improving modeling of AEM data affected by IP, two case studies: 24th International Geophysical Conference and Exhibition, ASEG, Expanded Abstracts, 1–5.

Yang, D., and D. W. Oldenburg, 2012, Three-dimensional inversion of airborne time-domain electromagnetic data with applications to a porphyry deposit: Geophysics, **77**, no. 2, B23–B34, doi: 10.1190/geo2011-0194.1.